Wang et al. Nanoscale Research Letters (2015) 10:236
DOI 10.1186/s11671-015-0947-7

Nanoscale Research Letters
a SpringerOpen Journal

NANO EXPRESS Open Access

Synthesis of Pt_3Ni Microspheres with High Performance for Rapid Degradation of Organic Dyes

Min Wang[1†], Yushi Yang[1†], Jia Long[1], Zhou Mao[1], Tong Qiu[1], Qingzhi Wu[1] and Xiaohui Chen[2*]

Abstract

In this study, Pt_3Ni microspheres consisted of nanoparticles were synthesized without addition of surfactants via the solvothermal route. The obtained sample was characterized by X-ray diffraction (XRD), inductively coupled plasma-atomic emission spectrometer (ICP-AES), X-ray photoelectron spectroscopy (XPS), and field-emission scanning electron microscopy (FESEM). Furthermore, the catalytic performance of as-synthesized Pt_3Ni microspheres was evaluated on the degradation of different organic dyes (methylene blue, methyl orange, Congo red, and rhodamine B). The results show that different dyes were rapidly decomposed by Pt_3Ni microspheres in different pathways. Among different dyes, the formation and further degradation of the intermediates was observed during the degradation of methylene blue and methyl orange, suggesting the indirect degradation process of these dyes. This study provides not only a promising catalyst for the removal of organic contaminants for environment remediation, but also new insights for Pt_3Ni alloy as a high-performance catalyst in organic synthesis.

Keywords: Pt_3Ni alloy; Catalytic degradation; Organic dye

Background

Organic dyes are typical water pollutants as the by-products of modern textile industry, which result in the breakdown of water ecosystem and greatly threaten the public health because they are potentially carcinogenic and cause various chronic diseases [1–3]. Therefore, the degradation of organic dyes is of great emergency in environment remediation. Various strategies, including physical adsorption [4–6], chemical degradation [7–9], and biodegradation by the microorganisms [10–12], have been developed for decomposing organic dyes from textile effluent. However, these methods are limited with different shortcomings, such as harsh degradation conditions, membrane fouling, low degradation efficiency, and extra post-treatment of sludge [13–16]. PtNi alloy has been proved as a catalyst with high performance for oxygen-reduction reaction [17] and methanol oxidation [18, 19]. Recent studies also demonstrated promising applications of PtNi nanoparticles (NPs) in the detection of glucose from human urine [20], hydrolytic hydrogenation of cellulose [21], catalytic reforming of ethanol, acetone, and methane [22–24]. The exceptionally high catalytic performance of PtNi could be attributed to the reduction of adsorption energy of the reaction intermediates and the increase of active sites on the surfaces of the catalyst when Pt was alloyed with 3d transition metals [25, 26].

In this study, Pt_3Ni microspheres consisting of NPs were synthesized via a facile solvothermal route without addition of the surfactants. The as-synthesized sample was characterized through X-ray diffraction (XRD), field-emission scanning electron microscopy (FESEM), high-resolution transmission electron microscopy (HRTEM), X-ray photoelectron spectroscopy (XPS), and inductively coupled plasma-atomic emission spectrometer (ICP-AES). Furthermore, the catalytic performance of Pt_3Ni microspheres was evaluated on the degradation of different dyes, including methylene blue (MB), methyl orange (MO), Congo red (CR), and rhodamine B (Rh-B). The results showed that the Pt_3Ni microspheres displayed high performance for catalytic degradation of different dyes through

* Correspondence: christinechen@aliyun.com
†Equal contributors
[2]Department of Prosthetic, School of Stomatology, Wuhan University, Wuhan 430079, People's Republic of China
Full list of author information is available at the end of the article

an alternative mechanism evidenced by the presence of the intermediates.

Methods

Synthesis of Pt_3Ni microspheres

In a typical synthesis, platinum acetylacetonate ($Pt(acac)_2$, 0.25 mmol, Sigma-Aldrich) was added into 20 mL ethylene glycol with magnetic stirring, which was heated to ca. 80 °C to ensure the completed dissolution of platinum salt. Then, $NiSO_4 \cdot 6H_2O$ (0.25 mmol, Sinopharm Chemical Reagent Co., Ltd.) was added into another 20 mL ethylene glycol with magnetic stirring. Then, the solution containing platinum salt was added into the $NiSO_4$ solution dropwise under magnetic stirring. Subsequently, the mixed solution containing metal salts was transferred into a 50 mL Teflon-lined stainless-steel autoclave and heated to 180 °C for 10 h, and then cooled to room temperature. The precipitate was collected and washed alternately with ethanol and deionized water by centrifugation (9000 rpm, 5 min), and then dried at 60 °C in vacuum.

Characterizations of Pt_3Ni microspheres

Phase structure of the as-obtained sample was characterized through X-ray diffraction (XRD, PANalytical X'Pert PRO, Holland) using Cu Kα radiation. The morphology of the sample was observed using a field-emission scanning electron microscopy (FESEM, Hitachi S-4800), and high-resolution transmission electron microscopy (HRTEM, JEM-2100 F STEM/EDS, JEOL Corp, Japan). X-ray photoelectron spectroscopy (XPS) measurement was performed on a VG Multilab 2000 (Thermo Electron Corp., MA) spectrometer using Al Kα radiation as the excitation source. An Optima 4300 DV inductively coupled plasma-atomic emission spectrometer (ICP-AES, Optima 4300DV Perkin-Elmer Corp.) was used to determine the elemental composition of the product.

Catalytic degradation of different dyes by Pt_3Ni microspheres

The catalytic performance of Pt_3Ni microspheres was evaluated by monitoring the degradation of different dyes (MB, 8 mg/L; MO, 20 mg/L; CR, 32 mg/L; and Rh-B, 7 mg/L) using **ultraviolet–visible spectroscopy** (UV–vis). In a typical experiment, Pt_3Ni microspheres (20 mg) was added into 50 mL dye aqueous solutions. The suspension was magnetically stirred at room temperature. The supernatants of the suspensions was collected and centrifuged (12,000 rpm, 5 min) at different time intervals (0, 5, 10, 20, 40, 60, 120, 180, 240 min). Afterwards, the supernatants were collected, and the changes of UV–vis absorption spectra were recorded on a UV–vis spectrophotometer (Shimadzu Corp., UV-2550 PC). In order to determine the degradation capacity of dyes catalyzed by Pt_3Ni microspheres, the degradation of MB was measured at different concentrations (2, 4, 8, 12, 16 mg/L).

Results and discussion

Figure 1 shows the FESEM and transmission electron microscope (TEM) images of the sample. As shown in Fig. 1a–c, irregular microspheres were obtained, which consisted of numerous NPs with an average diameter of ca. 50 nm. The assembly of NPs into microspheres was further confirmed by TEM observations (Fig. 1d–f). The well-aligned planes were observed by HRTEM characterization, as shown in the inset in Fig. 1f, indicating the single crystal nature of the as-synthesized sample. The interplanar distance was ca. 0.222 nm, which could be indexed to the adjacent (111) planes of the Pt_3Ni crystal.

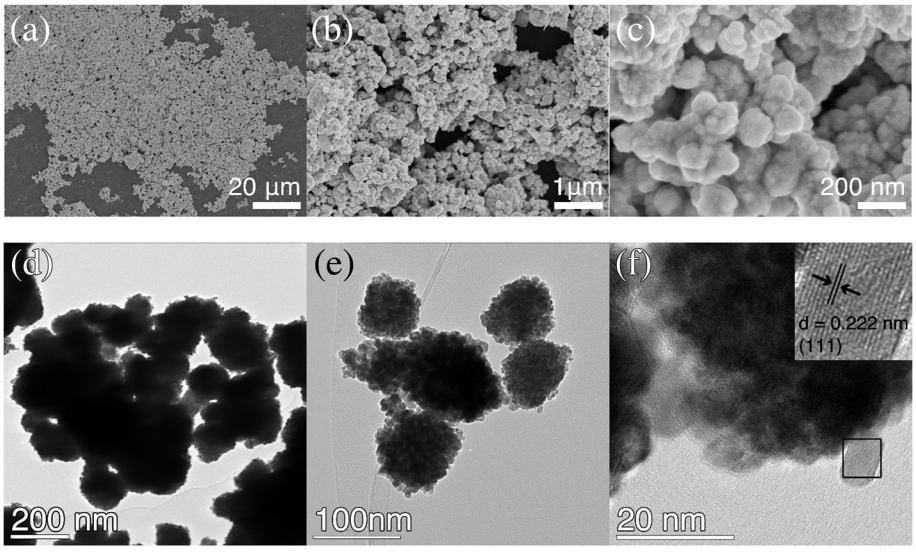

Fig. 1 FESEM and TEM images of the as-synthesized sample. **a**–**c** FESEM images of the sample; **d**–**f** TEM images of the sample

Figure 2 shows an XRD pattern of the as-synthesized Pt_3Ni microspheres. All diffraction peaks could be assigned to a cubic fcc structure. It was noteworthy that all diffraction peaks shifted to a higher 2θ degree compared with those of cubic Pt metal (JCPDS 70–2057), indicating a lower cell length. In order to obtain the cell length, Rietveld refinement was applied to fit the XRD data using Maud software [27]. As shown in Fig. 1, the cell length was ca. 3.850 Å after the refinement, smaller than that of Pt crystal (3.923) and larger than that of Ni crystal (3.523) [28]. This result indicates the incorporation of Ni atoms into the Pt crystal and therefore the formation of PtNi alloy. ICP-AES measurement further confirmed the presence of both Ni and Pt in the sample. The molar/weight percentage of Pt and Ni in the sample was ca. 66.97 and 33.03 %, respectively, suggesting the molar ratio of Pt/Ni was 3/1.

Figure 3 shows the XPS spectra of the as-synthesized Pt_3Ni microspheres. In Fig. 3a, the fitted peaks at ca. 71.1 and 75.1 eV could be ascribed to $4f_{7/2}$ and $4f_{5/2}$ spin orbit of Pt^0 [18]. The XPS spectrum of Ni was fitted with Gaussian functions by a least-square procedure provided by Numpy and SciPy packages [29]. As shown in Fig. 3b, the fitted peaks at ca. 852, 856, 859 eV and 870, 874, 880 eV could be ascribed to $2p_{5/2}$ and $2p_{3/2}$ spin orbit of Ni^0, Ni^{2+}, and their satellite peaks, respectively. The oxidation of Ni might be related to its contact with air. These results further confirmed the formation of Pt_3Ni alloy.

In order to evaluate the catalytic performance of Pt_3Ni microspheres, the degradation of different dyes was determined by monitoring the changes of UV–vis spectra. Figure 4 shows the UV–vis spectra of different dye solutions (MB, MO, Rh-B, and CR) treated with 20 mg Pt_3Ni microspheres for different times. It is of great interest

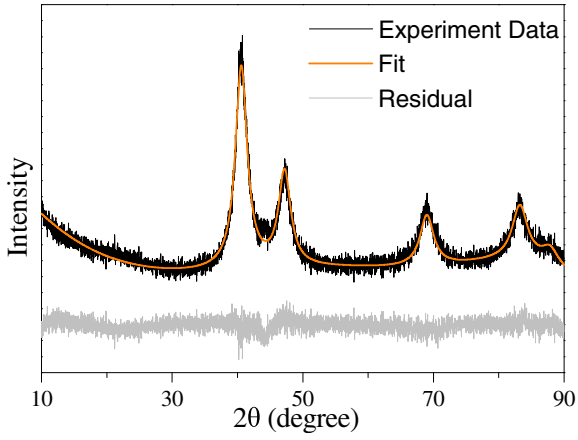

Fig. 2 XRD pattern of the as-synthesized Pt_3Ni microspheres. The *fitted line* and the residual showed the result of the Rietveld refinement. The cell length after refinement was ca. 3.85 Å, lower than that of Pt and larger than that of Ni

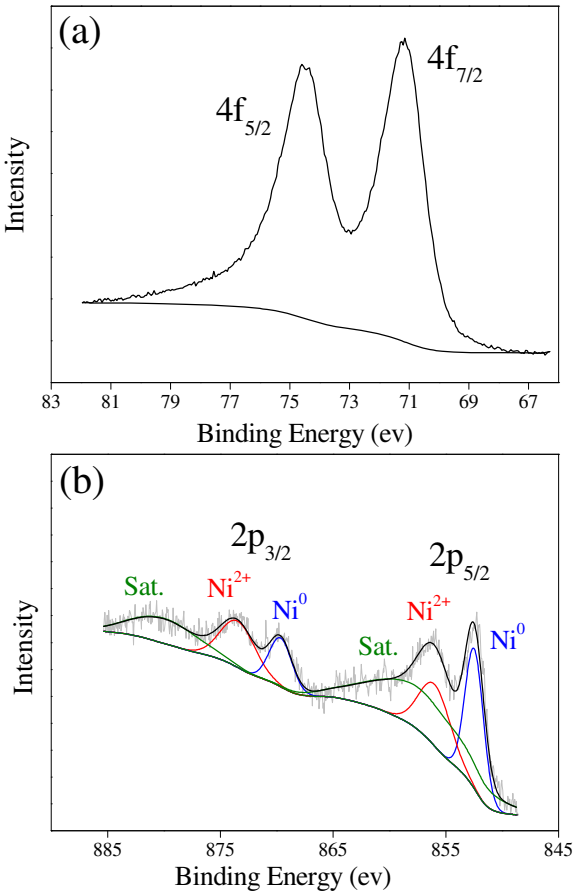

Fig. 3 XPS spectra of Pt 4f (**a**) and Ni 2p (**b**) of the as-obtained Pt_3Ni microspheres

that different degradation processes were observed among the four dyes used. As shown in Fig. 4a and b, a series of new absorption peaks appeared immediately in UV–vis spectra of MB and MO solution after 5 min of treatment, indicating the formation of the intermediates. On the other hand, as shown in Fig. 4c and d, the absorption peaks derived from Rh-B and CR were gradually decreased after the treatment with Pt_3Ni microspheres without the presence of new absorption peaks, suggesting the direct degradation of Rh-B and CR by Pt_3Ni microspheres.

In order to explore the relationship between the degradation of MB and the formation of the intermediates, a series of fittings were performed on the UV–vis spectra of MB solution treated with Pt_3Ni microspheres for different times using a least-square procedure provided by Numpy and SciPy packages [29]. The fittings were set in the wavelength range between 350 to 800 nm for simplification. The spectrum of pure MB solution was firstly fitted with several Gaussian functions. The obtained fitting result represented the profile of MB and was subsequently used for fitting the UV–vis spectra of MB solution treated with Pt_3Ni microspheres for different

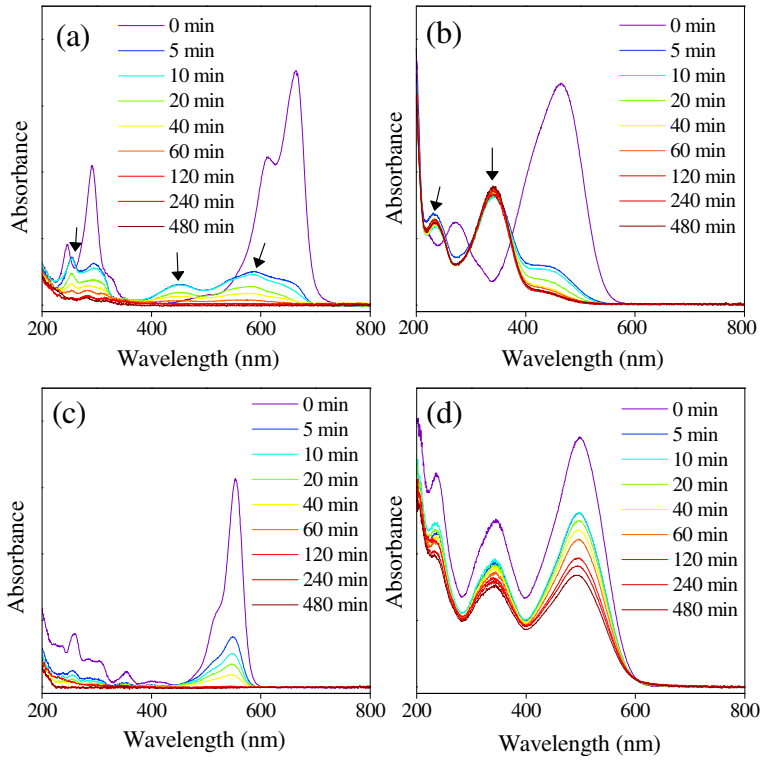

Fig. 4 UV–vis spectra of different dye solutions treated with Pt_3Ni microspheres for different times. **a** MB, 8 mg/L; **b** MO, 20 mg/L; **c** Rh-B, 7 mg/L; **d** CR, 32 mg/L. The absorption peaks of the intermediates were pointed out by the *arrows* in (**a**) and (**b**)

times (5, 10, 20, 40, 60, 120, 180, 240, and 1440 min). Figure 5 shows the fitting results of the UV–vis spectra of MB solution at an initial concentration of 16 mg/L. It was obvious that the absorption peaks derived from the intermediates appeared after 5 min of treatment. The absorption intensities derived from the intermediates increased at the initial stage and then decreased gradually. The absorption peaks derived from MB completely vanished after 120 min of treatment, whereas the absorption peaks derived from the intermediates completely vanished after 1440 min of treatment.

The similar fittings were also performed on the UV–vis spectra of MB solutions at different initial concentrations (2, 4, 8, and 12 mg/mL). The degradation of MB and the formation of the intermediates were further compared by relating the absorption intensity with the

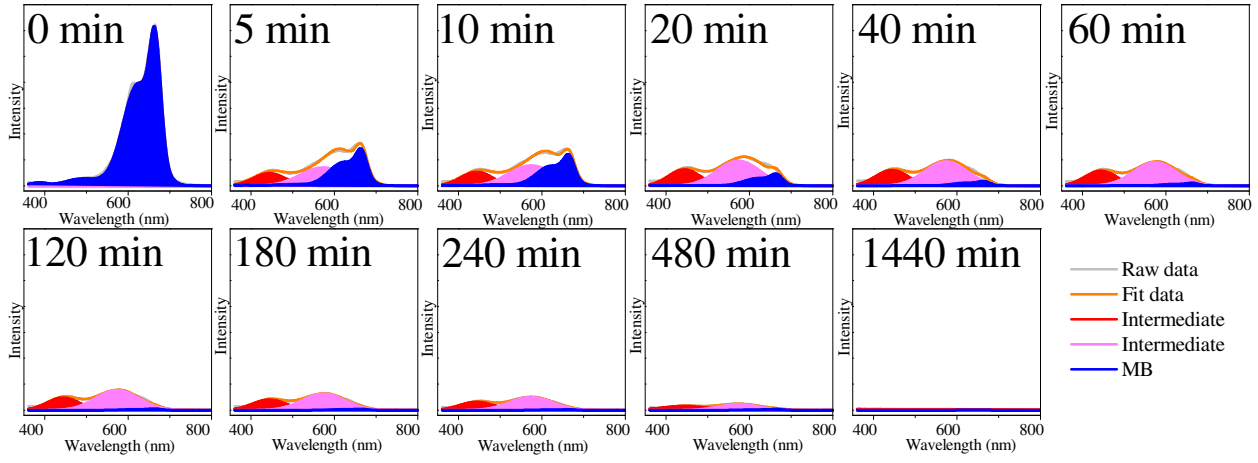

Fig. 5 UV–vis spectra fittings of MB solution (16 mg/L) treated with Pt_3Ni microspheres for different times

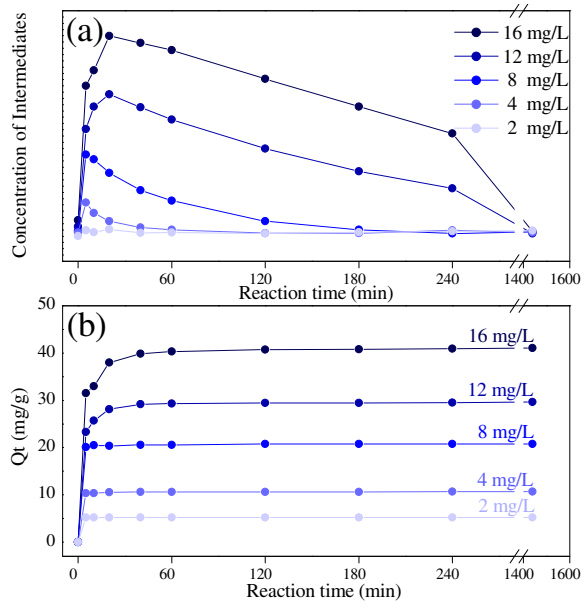

Fig. 6 The degradation of intermediates at different initial concentrations of MB. **a** The absorption intensity derived from the intermediates (the *red* and *blue* fitting peak) as shown in Fig. 5 was summed and supposed to be proportional to the concentration of the intermediates; **b** The degradation efficiency (Q_t) of the Pt_3Ni microspheres on MB dye with various initial MB concentrations

concentration. The intensity of absorption peaks derived from the intermediates (both the red and blue fitting peak as shown in Fig. 5) was summed and indexed as the concentration of the intermediates.

Figure 6a shows the formation and degradation of the intermediates at different initial concentrations of MB solution treated by Pt_3Ni microspheres. It was obvious that the concentration of the intermediates was sharply increased at the initial stage of treatment and subsequently decreased gradually. The completed degradation of the intermediates was dependent on the initial concentration of MB, which finished within 4 h at the MB concentration lower than 8 mg/mL and within 24 h at the MB concentration higher than 12 mg/mL. Figure 6b shows the degradation efficiency (Q_t) of the Pt_3Ni microspheres on MB dye at different initial concentrations. The degradation efficiency of Pt_3Ni microspheres was calculated as follows:

$$Q_t = (C_0 - C_t) * V/m$$

Where, C_0 and C_t are the concentrations of the MB solution at the initial and different time intervals; V is the volume of the reaction system (i.e., 50 mL); m is the weight of the Pt_3Ni microspheres used; and Q_t represents the weight of the MB absorbed/degraded per-unit weight of Pt_3Ni microspheres. At a low initial concentration (2, 4, and 8 mg/mL) of MB, Q_t value was sharply increased and rapidly reached the balance corresponding to the 100 % degradation of MB. However, at a higher initial concentration (12 and 16 mg/mL) of MB, the changes of Q_t value were slower, suggesting that the degradation rate of MB was decreased due to the increase of MB concentration. Therefore, these results implied that the degradation of MB may occur on the surface of Pt_3Ni NPs.

As observed in the fitted UV–vis spectra, the absorption peaks derived from the intermediates shifted to the shorter wavelength compared with that of MB, implying that the smaller conjunction system contained in the intermediates than that of in MB molecular [30, 31]. In addition, the previous studies also revealed that the aromatic molecules could be adsorbed on the surfaces of both Pt and Ni [32–36]. Therefore, it is speculated that the catalytic degradation of MB molecules involved the adsorption of MB molecules on the surfaces of Pt_3Ni NPs, the subsequent formation and degradation of the intermediates on the active sites of Pt_3Ni NPs. More investigations are being undergone to explore the precise formation and degradation mechanisms of the intermediates during the catalytic degradation of MB by Pt_3Ni NPs.

Conclusions

In summary, Pt_3Ni microspheres consisting of nanoparticles were successfully synthesized via a facile route without addition of the surfactants. The as-synthesized Pt_3Ni microspheres displayed high performance for the catalytic degradation of various organic dyes. The results showed that the degradation of MB and MO by Pt_3Ni microspheres was involved in the formation of the intermediates. These results not only provide a promising catalyst for the removal of organic contaminants for environment remediation, but also provide new insights for Pt_3Ni alloy as a high-performance catalyst in organic synthesis.

Competing interests

The authors declare that they have no competing interests.

Authors' contributions

MW and YY carried out the synthesis and characterization of Pt_3Ni microspheres, JL and ZM participated in the measurement of degradation of different dyes by Pt_3Ni. YY, TQ, and QW analyzed the data, and drafted the manuscript. XC and QW designed the whole work and revised the manuscript. All authors read and approved the final manuscript.

Acknowledgements

This work was financially supported by the Natural Science Foundation of China (No. 30800256 and 31300791), the basic research project of Wuhan Science and Technology Bureau (No. 2014060101010041), and the Key Grant Project of Chinese Ministry of Education (No. 313041).

Author details

[1]State Key Laboratory of Advanced Technology for Materials Synthesis and Processing, Wuhan University of Technology, Wuhan 430070, People's

Republic of China. [2]Department of Prosthetic, School of Stomatology, Wuhan University, Wuhan 430079, People's Republic of China.

Received: 2 April 2015 Accepted: 20 May 2015
Published online: 27 May 2015

References

1. Slokar YM, Le Marechal AM. Methods of decoloration of textile wastewaters. Dyes Pigments. 1998;37(4):335–56.
2. Weisburger JH. Comments on the history and importance of aromatic and heterocyclic amines in public health. Mutat Res. 2002;506–507:1–12.
3. Strickland AF, Perkins WS. Decolorization of continuous dyeing wastewater by ozonation. Text Chem Color. 1995;27(5):11–5.
4. Gan Y, Tian N, Tian X, Ma L, Wang W, Yang C, et al. Adsorption behavior of methylene blue on amine-functionalized ordered mesoporous alumina. J Porous Mater. 2014;22(1):147–55.
5. Zhu X, Zheng Y, Chen Z, Chen Q, Gao B, Yu S. Removal of reactive dye from textile effluent through submerged filtration using hollow fiber composite nanofiltlration membrane. Desalin Water Treat. 2013;51(31–33):6101–9.
6. Sonar SK, Niphadkar PS, Mayadevi S, Joshi PN. Preparation and characterization of porous fly ash/NiFe2O4 composite: promising adsorbent for the removal of congo red dye from aqueous solution. Mater Chem Phys. 2014;148(1–2):371–9.
7. Zhai C, Zhu M, Bin D, Wang H, Du Y, Wang C, et al. Visible-light-assisted electrocatalytic oxidation of methanol using reduced graphene oxide modified Pt nanoflowers-TiO2 nanotube arrays. ACS Appl Mater Interfaces. 2014;6(20):17753–61.
8. Zodi S, Merzouk B, Potier O, Lapicque F, Leclerc J-P. Direct red 81 dye removal by a continuous flow electrocoagulation/flotation reactor. Sep Purif Technol. 2013;108(C):215–22.
9. Mao Z, Wu Q, Wang M, Yang Y, Long J, Chen X. Tunable synthesis of SiO2-encapsulated zero-valent iron nanoparticles for degradation of organic dyes. Nanoscale Res Lett. 2014;9(1):501.
10. Chen SH, Ting ASY. Biodecolorization and biodegradation potential of recalcitrant triphenylmethane dyes by Coriolopsis sp isolated from compost. J Environ Manag. 2015;150(c):274–80.
11. Han Y, Shi L, Meng J, Yu H, Zhang X. Azo dye biodecolorization enhanced by Echinodontium taxodii cultured with lignin. PLoS One. 2013;9(10):e109786.
12. McMullan G, Meehan C, Conneely A, Kirby N, Robinson T, Nigam P, et al. Microbial decolourisation and degradation of textile dyes. Appl Microbiol Biotechnol. 2001;56(1–2):81–7.
13. Thamaraiselvan C, Noel M. Membrane processes for dye wastewater treatment: recent progress in fouling control. Crit Rev Environ Sci Technol. 2015;45(10):1007–40.
14. Saratale RG, Saratale GD, Chang JS, Govindwar SP. Bacterial decolorization and degradation of azo dyes: a review. J Taiwan Instit Chem Eng. 2011;42(1):138–57.
15. Brillas E. A Review on the degradation of organic pollutants in waters by UV photoelectro-fenton and solar photoelectro-fenton. J Braz Chem Soc. 2013: 1–25. http://www.scielo.br/pdf/jbchs/v25n3/a02v25n3.pdf
16. Vandevivere PC, Bianchi R, Verstraete W. Review: treatment and reuse of wastewater from the textile wet processing industry: review of emerging technologies. J Chem Technol Biotechnol. 1998;72(4):289–302.
17. Matanović I, Garzon FH, Henson NJ. Theoretical study of electrochemical processes on Pt–Ni alloys. J Phys Chem C. 2011;115(21):10640–50.
18. Nassr ABAA, Sinev I, Pohl M-M, Grünert W, Bron M. Rapid microwave-assisted polyol reduction for the preparation of highly active Pt3Ni/CNT electrocatalysts for methanol oxidation. ACS Catal. 2014;4(8):2449–62.
19. Luo B, Xu S, Yan X, Xue Q. Synthesis and electrochemical properties of graphene supported Pt3Ni nanodendrites. Electrochem Commun. 2012;23(C):72–5.
20. Gao H, Xiao F, Ching CB, Duan H. One-step electrochemical synthesis of Pt3Ni nanoparticle-graphene nanocomposites for nonenzymatic amperometric glucose detection. ACS Appl Mater Interfaces. 2011;3(8):3049–57.
21. Liang G, He L, Arai M, Zhao F. The Pt-enriched Pt3Ni alloy surface and its excellent catalytic performance in hydrolytic hydrogenation of cellulose. ChemSusChem. 2014;7(5):1415–21.
22. Moraes TS, Neto RCR, Ribeiro MC, Mattos LV, Kourtelesis M, Ladas S, et al. The study of the performance of Pt3Ni/CeO2–nanocube catalysts for low temperature steam reforming of ethanol. Catal Today. 2015;242:35–49.
23. Navarro RM, Guil-Lopez R, Ismail AA, Al-Sayari SA, Fierro JLG. Ni- and Pt3Ni-catalysts supported on Al2O3 for acetone steam reforming: effect of the modification of support with Ce. La Mg Catalysis Today. 2015;242:60–70.
24. de Miguel SR, Vilella IMJ, Maina SP, José-Alonso DS, Román-Martínez MC, Illán-Gómez MJ. Influence of Pt addition to Ni catalysts on the catalytic performance for long term dry reforming of methane. Appl Catal A Gen. 2012;435–436:10–8.
25. Lutterotti L, Chateigner D, Ferrari S, Ricote J. Texture, residual stress and structural analysis of thin films using a combined X-ray analysis. Thin Solid Films. 2004;450(1):34–41.
26. Kitchin JR, Nørskov JK, Barteau MA, Chen JG. Modification of the surface electronic and chemical properties of Pt(111) by subsurface 3d transition metals. J Chem Phys. 2004;120(21):10240–8.
27. Chen D, Zhao X, Chen S, Li H, Fu X, Wu Q, et al. One-pot fabrication of FePt/reduced graphene oxide composites as highly active and stable electrocatalysts for the oxygen reduction reaction. Carbon. 2014;68(C):755–62.
28. Swanson HE, Tatge E. Standard X-ray diffraction powder patterns, vol. I. Washington, D.C.: National Bureau of Standards; 1953.
29. Millman J, Vaught T. The State of SciPy. In: Varoquaux el G, Vaught T, Millman J, editors. Pasadena, CA USA; 2008. p. 5–10.
30. Hao L, Wang W, Sun Y, Niu H. Synthesis and electrochromic properties of novel poly(urethane–azomethine)s containing triphenylamine units. J Electroanal Chem (Lausanne Switz). 2015;742:74–83.
31. Zhou J, Yu X, Jin X, Tang G, Zhang W, Hu J, et al. Novel carbazole-based main chain polymeric metal complexes containing complexes of phenanthroline with Zn(II) or Cd(II): synthesis, characterization and photovoltaic application in DSSCs. J Mol Structure. 2014;1058(C):14–21.
32. Yang J, Dauenhauer PJ, Ramasubramaniam A. The role of water in the adsorption of oxygenated aromatics on Pt and Pd. J Comput Chem. 2012;34(1):60–6.
33. Saeys M, Reyniers M-F, Marin GB, Neurock M. Density functional study of benzene adsorption on Pt(111). J Phys Chem B. 2002;106(30):7489–98.
34. Sautet P, Bocquet ML. Shape of molecular adsorbates in STM images: a theoretical study of benzene on Pt(111). Phys Rev B. 1996;53(8):4910–25.
35. Site LD, Leon S, Kremer K. Specific interaction of polymers with surface defects: structure formation of polycarbonate on nickel. J Phys Condens Matter. 2005;17(4):L53–60.
36. Mittendorfer F, Hafner J. Hydrogenation of benzene on Ni(111)a DFT study. J Phys Chem B. 2002;106(51):13299–305.